The World's Largest Point Rainfall Found Using the Precipitation Intensity Duration Index

RASMUS WIUFF[a]

[a] *Virum, Denmark*

(Manuscript received 21 January 2023, in final form 16 July 2023, accepted 4 August 2023)

ABSTRACT: World extremes in meteorology are important as they can be used as indicators for climate change. This was one of the main reasons for the creation of the World Meteorological Organization's World Weather and Climate Extremes Archive in 2006. In contrast to temperature, for instance, which can be described by a single parameter, point rainfall must be described by two parameters, for example, precipitation depth and duration. This makes it difficult to directly compare different rainfall records. In this article, however, it is shown that the world's greatest rainfall events, with durations ranging from 1 min to 2 years, all have nearly the same precipitation intensity duration index, a new dimensionless number. As a theoretical consequence, the intensity of all these record rainfalls is inversely proportional to the square root of their duration. This physically based result is consistent with earlier statistically based findings. The last measured record rainfall on the World Meteorological Organization's record list is the point rainfall with the largest precipitation intensity duration index since 1860. This 4-day rainfall that began on 24 February 2007 on Cratère Commerson, Réunion Island, can be considered the largest point rainfall within documented records.

SIGNIFICANCE STATEMENT: Floods resulting from extreme rainstorms can be very costly and deadly; thus, understanding such extreme events is very important. Knowledge of extreme rainstorms is also important in determining how much and how fast our climate is changing. In this article, a new dimensionless number, the precipitation intensity duration index (PID) is presented. The world's greatest point rainfall events, with durations ranging from 1 min to 2 years, all have nearly the same PID. One rainfall event, however, has a considerably larger PID than all others, namely, a 4-day rainfall that began on 24 February 2007 on Cratère Commerson, Réunion Island. Therefore, this rainfall can be considered the largest point rainfall within documented records.

KEYWORDS: Atmosphere; Precipitation; Rainfall; Severe storms; Ranking methods

1. Introduction

Floods resulting from extreme rainstorms can be very costly and deadly; thus, understanding such extreme events is very important. Knowledge of weather and climate extremes is also important in determining how much and how fast our climate is changing, as stated by Randy Cerveny, the World Meteorological Organization's rapporteur for Extreme Records (Cerveny 2018). In 2006, therefore, the World Meteorological Organization (WMO) Commission for Climatology (CCI) decided to create a world archive for verified and certified weather extremes (WMO 2023). A set of procedures was established such that existing and future weather record extremes could be verified and made available to the general public. Since then, an official, certified, and verified list of weather extremes has been presented in the WMO Global Weather and Climate Extremes Archive (WMO 2023). This archive comprises world records of temperature, pressure, rainfall, and so forth. All WMO records are the directly measured instrument values without corrections (i.e., readings of thermometer, rain gauge, clock). Some weather records are simple numbers; for instance, the highest and lowest temperatures ever recorded are, incidentally, 56.7° and −89.2°C, respectively (WMO 2023). Other world records are more complicated, for instance, those about rainfall, because a measured rainfall depth is relevant only if it is related to the duration of the rainfall. In this way, there could be many world records, with durations ranging from a few seconds to several years. At present, the WMO's archive is limited to only eight rainfall records.

The main purpose of this analysis is to clarify whether it is possible to identify one of these eight rainfalls as the largest. A method, therefore, must be found that makes it possible to compare rainfalls with different depths and different durations. There exist several methods for describing rainfall that may be used for comparing different rainfalls. The basic measurement, or the primary parameter, is the total amount of precipitation expressed in depth of water that reaches the ground in a stated period (WMO 2021). In this way, rainfalls with long durations are the largest, which, for the present analysis, is not interesting. Normally, the period is fixed time intervals, for example, 1 min or 1 day. The intensity is the amount of precipitation collected per time interval, that is, the

Denotes content that is immediately available upon publication as open access.

Wiuff: Retired.

Corresponding author: Rasmus Wiuff, rasmus.wiuff@gmail.com

DOI: 10.1175/JHM-D-23-0012.1

intensity is a secondary parameter, although intensity can also be measured directly (WMO 2021). A single rainfall incident can be described by the time series of the intensity and compared with other time series, or the maximum intensity can be derived and compared to other maximum intensities. In this way, rainfalls with the shortest time intervals will win, which, again, is not interesting.

A single rainfall can also be described by the maximum intensities for different time intervals, leading to an intensity–duration (ID) table or an ID curve, which makes it possible to compare different rainfalls, but only if they have overlapping durations. This is, in principle, the way in which the WMO (2023) found the eight world records. If all rainfall intensities and related durations from several years within a limited area are treated, as they often are, by means of extreme value theory, the so-called ID frequency (IDF) relationship can be established. The pioneering work goes back to Bernard (1932), who presented rainfall intensities for return periods (average recurrence intervals) from 5 to 100 years for durations from 2 to 100 h. Since then, IDF relationships have played an important role in planning and designing various engineering projects, such as dams, spillways, storm sewers, and culverts for highways. IDF relationships have been presented as tables, curves, and mathematical equations (see, e.g., Keifer and Chu 1957; Wenzel 1982; Chow et al. 1988; Koutsoyiannis et al. 1998; Koutsoyiannis and Papalexiou 2017; Johnson and Sharma 2017; Sun et al. 2019; Gámez-Balmaceda et al. 2020; Koutsoyiannis 2022). To avoid overdesign, areal reduction factors (ARFs) have been introduced (see, e.g., Rosbjerg and Madsen 2019). It should be emphasized that in the present analysis, the effect of areal extent has not been analyzed, as only point rainfalls are studied. In the discussion, some options have been outlined for extending the analysis to include areas and not just points.

Martel et al. (2021) used IDF relationships to analyze climate change. With reliable IDF relationships, it is possible to find the frequencies or return periods for different time intervals of a given rainfall incident, which could appropriately be called tertiary parameters. The minimum frequency or the maximum return period (the recurrence interval) found in this way is a unique characteristic of this rainfall, which can be compared with other rainfalls to pinpoint the largest rainfall. Today, IDF relationships exist for most areas of several countries, such as the United States (NOAA 2023), Australia (Bureau of Meteorology 2023), Germany (DWD 2022), and Denmark (Gregersen et al. 2014). An IDF relationship is, however, related to a specific area. Therefore, generally, for example, a 100-yr incident from a certain area in the United States can be very different from a 100-yr incident from some place in Denmark. For that reason, it is not useful directly to compare world records using IDF relationships or return periods, as will be illustrated in the analysis.

If one goes even further back in the "parameter hierarchy," it may be possible to compare rainfall events from different places around the world, inclusive of the world records. Unfortunately, the problem seems not to be solved by comparing other tertiary parameters stemming from widely used methods such as probable maximum precipitation (PMP) (WMO 2009a; Mukhopadhyay and Kappel 2017), time series models involving Markov models and autoregressive moving average (ARMA) models (Gabriel and Neumann 1962; Caskey 1963; Chang et al. 1984; Katz and Parlange 1998; Schoof and Pryor 2008; Hannachi 2012; Lombardo et al. 2017; Wiuff 2020), and models based on artificial neural networks (Dahamsheh and Aksoy 2009) or entropy theory (Koutsoyiannis 2006).

However, a recent work by Koutsoyiannis (2022) describes how IDF curves are basically related to the probability distribution function (pdf) of precipitation. In this way, the empirical equations can be linked to the pdf of the precipitation process and thus to its stochastic structure and not only to some empirical expressions. Koutsoyiannis (2004a,b, 2005) showed that theoretical arguments and analyses of many rainfall records worldwide point to extreme value type 2 (EV2; or Fréchet distribution) as the best extreme value probability distribution to describe extreme rainfall maxima, that is, better than the previous prevailing model, the Gumbel distribution. Koutsoyiannis and Papalexiou (2017) found that the shape parameter of the EV2 distribution varied only in a relatively narrow range worldwide, but there was still too much variation to pinpoint a single rainfall as the largest event. However, if EV2 is used to generate extreme rainfall records, no persistence will occur. This is in contrast to the findings of Iliopoulou and Koutsoyiannis (2019), who showed that maximum rainfall exhibits the Hurst phenomenon, that is, long-range dependence. A solution to this is to generate the whole parent process (not just the extreme tail) of precipitation by including both the pdf and autocorrelation function with persistence of the precipitation process (Koutsoyiannis 2000, 2016, 2020a). The method of preserving both the pdf and the autocorrelation function, and not just using them implicitly through transformations, as in copula and other transformation models (see e.g., Grimaldi and Serinaldi 2006; Genest and Chebana 2017; Papalexiou 2018) has addressed the limitations of such transformation models, for instance, regarding long-range dependence. A comprehensive review on generating methods for precipitation and other hydrological models was recently provided by Beven (2021). For the parent pdf, Koutsoyiannis (2022) has newly proposed the so-called Pareto–Burr–Feller distribution together with a mixed fractal and long-range persistence autocorrelation function. With this parameterization it is possible to compare different extreme records from different sites around the world. Dimitriadis et al. (2021) have performed a global-scale investigation of stochastic similarities in marginal distribution and dependence structure of the precipitation process, showing that although rainfall extremes magnitudes and durations may differ from site to site, if they are viewed through the dimensionless parameters of the pdf and autocorrelation function, then analogies can be extracted that allow a unified view of not only the precipitation structure but also other key water-cycle processes, such as temperature, wind speed, humidity, and dewpoint.

In this analysis, however, a quite different approach than that described above has been used, namely, dimensional analysis. In this way, only primary and secondary parameters have to be used, making the analysis very simple. The parameter

estimation is independent of geographic location, making it possible to compare point rainfalls all over the world. For the analysis, more than the eight rainfall events (WMO 2023) are needed to obtain better coverage of the different durations and to reveal, if possible, their temporal development. Therefore, the WMO list from 2023 is supplemented by older lists of records (Jennings 1950; NOAA 2021; U.S. Weather Bureau 1941; WMO 2009b). The WMO list from 2023 covers durations from 1 min to 1 year, with rainfall depths ranging from 31.2 mm to 26.47 m. This is truly a large span, and one could ask if these events, on the whole, have anything in common. Observations of rainfall records are often depicted by applying the logarithmic value of the depth or the intensity versus the logarithmic value of the duration, resulting in a nearly linear relation (Jennings 1950; Koutsoyiannis and Papalexiou 2017; NOAA 2021; U.S. Weather Bureau 1941). This simple but only statistically based relation has never been provided with a physical interpretation. By applying dimension analysis, a physically based relationship between the depth or the intensity versus the duration of rainfall is provided. This shows that the world's greatest point rainfalls do have something in common. Based on these findings, it is possible to appoint one single rainfall incident as the world's greatest point rainfall event within documented records. This means that this rainfall event is greater than all the others, independent of their duration.

2. Theory

The physics of extreme rainfall events are very complicated and difficult to simulate due to both the need for extremely high computer power and the complex physical processes. Dimensional analysis, however, is a simple tool to obtain insight into complicated physical problems where the use of classical methods is too difficult (Hecksher 2017). Dimensional analysis has been used for more than 100 years with success in many different subject areas, such as in turbulent flows by Reynolds (1883) and in atomic physics by Bohr (1913). Beard (1976) also used dimensional analysis in his assessment of the terminal velocity of cloud and precipitation drops.

A dimensional analysis is used to identify possible dimensionless numbers describing important features regarding extreme rainfall events. The Buckingham π theorem (Buckingham 1914) states that if there are q physical quantities in a problem and these quantities have p dimensions (e.g., mass, length, time), then the problem can be described by $q - p$ independent, dimensionless parameters or numbers.

Dimensional analysis requires a qualified estimate of the quantities relevant to the physical problem at hand. The present analysis examines the relation between point precipitation and duration. Precipitation depth n has the dimension of length, while duration t has the dimension of time. As these two quantities have different dimensions, other quantities must be included to achieve dimensionless numbers.

The formation of clouds and the subsequent formation of rain depend on many conditions, such as solar radiation and water condensation. To avoid introducing more dimensions than those already present, length and time, the analysis is limited to additional quantities with these two dimensions only. Here, it makes sense to include the gravitational acceleration g (m s^{-2}) and the kinematic viscosity of the air ν (m^2 s^{-1}), as they are both related to the physics of falling water droplets.

The four quantities, n, t, g, and ν, are now combined into dimensionless numbers. With four quantities and two dimensions, Buckingham's π theorem gives $4 - 2 = 2$ independent, dimensionless numbers. Many pairs of such dimensionless numbers can be found. Initially, it is appropriate to make the precipitation dimensionless by introducing a characteristic precipitation $n_0 = \nu^{2/3} g^{-1/3} = 2.62 \times 10^{-4}$ m and likewise for the time $t_0 = \nu^{1/3} g^{-2/3} = 5.17 \times 10^{-3}$ s. Here, $g = 9.81$ m s^{-2} and $\nu = 1.33 \times 10^{-5}$ m^2 s^{-1} (air at 0°C) are used.

Then, the dimensionless precipitation and the dimensionless time are

$$n' = n/n_0, \tag{1}$$

$$t' = t/t_0, \tag{2}$$

which are the first set of two independent dimensional numbers. The derived dimensionless intensity is obtained as $i' = n'/t' = i/i_0$, where $i_0 = n_0/t_0 = 5.07 \times 10^{-2}$ m s^{-1}. If i' is used, then either n' or t' must be omitted to maintain the number of independent dimensionless numbers at two.

Since no more information is obtained from depicting n' or i' as dependent on t' rather than n or i as dependent on t, which is the usual method of depiction, the dimensionless numbers n', t', and i' must be combined to obtain something useful and new. Examples of such combinations are the following two independent dimensionless numbers:

$$\mathrm{PID} = n'^2/t' = n^2/t\nu = in/\nu = i^2 t/\nu, \tag{3}$$

$$\mathrm{Fr} = n'^{1/2}/t = n^{1/2}/tg^{1/2} = i/(ng)^{1/2}. \tag{4}$$

The first dimensionless number, here called the precipitation intensity duration index (PID), has the same structure as a well-known and widely used dimensionless number in hydrodynamics and aerodynamics, namely, the Reynolds number (Re): $\mathrm{Re} = vl/\nu$, where v is the velocity, l is the length, and ν is the kinematic viscosity. The traditional Re expresses the relationship between the dynamic and viscous forces and can be used to determine whether a flow is laminar or turbulent, which Reynolds (1883) was the first to show.

However, this interpretation of (3) makes no sense in the case of rainfall. Here, it is necessary first to discuss what characterizes a severe rainstorm. Is it a short but very intensive cloudburst, or is it a very prolonged rainstorm with a substantial amount of precipitation? The answer to this question will depend on who is affected by the rainfall. In PID, the numerator is the product of these two decisive quantities, that is, the intensity times the amount of precipitation. Therefore, PID is a measure of the strength of the rainfall. As the quantities in PID have the same dimensions as the quantities in the well-known Reynolds number, it could have been named the "Reynolds rainfall number" in honor of Sir Reynolds. However, this could be confusing, which is why the more neutral name "precipitation intensity duration index" has been chosen. From (3), it is seen that

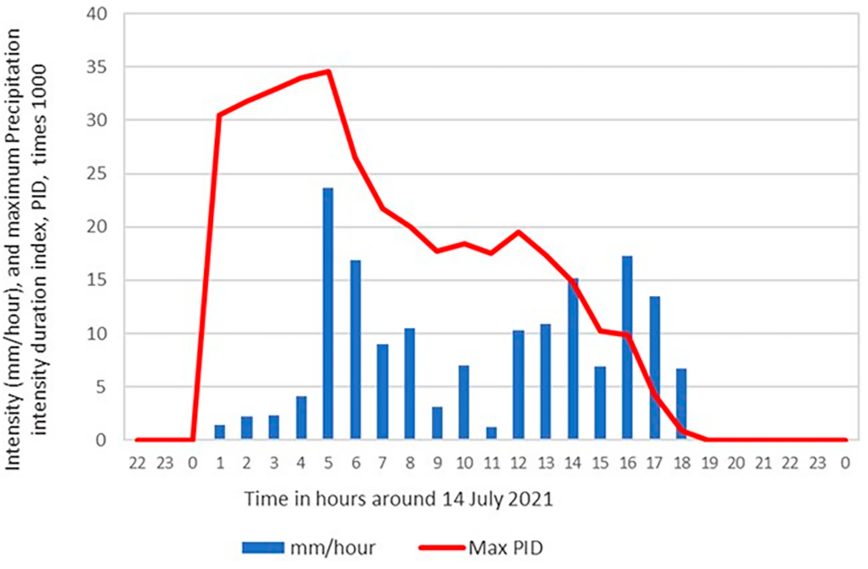

FIG. 1. Rainfall and maximum PID for each time step. Observations from 14 Jul 2021 at Wipperfürth-Gardeweg in the federal state of North Rhine-Westphalia, Germany (DWD 2023).

the PID can be expressed by precipitation depth and duration (PD), precipitation depth and intensity (PI), or intensity and duration (ID).

The second dimensionless number, Fr, Eq. (4), has the same structure as the Froude number F, which is also known from hydrodynamics and aerodynamics. The use of PID in combination with Fr does not yield useful additional results compared to the use of PID alone. Therefore, the dimensional analysis has been reduced to considering only the dimensionless PID. The dimensional analysis has shown that instead of describing rainfalls by two parameters (e.g., depth and duration), they can be described by one parameter, the precipitation intensity duration index.

For every point rainfall event worldwide, regardless of its precipitation depth and duration, it is possible to find a single maximum PID, which is a unique signature for this rainfall. Therefore, PID can be used to analyze and compare different rainfall events, for example, in time or space. The maximum PID for a point rainfall event is found as described below.

The rainfall starts at time zero and the total duration is t. The precipitation depth n_l is recorded every time step Δt, where Δt can be a minute, an hour, a day, and so on. The total number of precipitation records is $m = t/\Delta t$. Therefore, at time zero, is it possible to estimate m "sub-PID," starting with the first time step (length Δt); the first and the second time step (length $2\Delta t$); the first, the second, and the third time step (length $3\Delta t$); and ending with all m time steps (length $m\Delta t$). At time zero plus Δt, it is possible to estimate $m - 1$ sub-PID, starting with the second time step (length Δt), the second and the third time step (length $2\Delta t$), and ending with $m - 1$ time steps [length $(m - 1)\Delta t$]. This process continues until the last time step is considered (length Δt), resulting in a total of $m(m + 1)/2$ sub-PID, from which the maximum can be found:

$$\text{PID} = \text{max entry of } \mathbf{A}, \tag{5}$$

in which $\mathbf{A}$ is an $m \times m$ matrix with the following entries:

$$a_{j,k} = \left\{ \sum_{l=j}^{j+k-1} n_l/v \right\}^2 \Big/ k\Delta t \tag{6}$$

To illustrate the application of (5) and (6), data were used from the catastrophic rainfall in central Europe in July 2021, in which more than 200 people lost their lives in Germany and Belgium (DWD 2023; Magnusson et al. 2021). The analysis site, Wipperfürth-Gardeweg, is located approximately 30 km southeast of Wuppertal in the federal state of North Rhine-Westphalia. Here, the rainfall started just after midnight on 14 July and continued until approximately 2000 LT (see Fig. 1, where the rainfall per hour is shown along with the maximum PID found for each time step). The maximum of these maxima is PID = 0.0346, based on the 152.24 mm of precipitation recorded in the 14 h from 0500 to 1800 LT. If 10-min-long intervals are used instead, the maximum PID is 0.0348, based on the 152.65 mm recorded in the 14 h (coincidently, the same length as for the 1-h-long intervals) from 0450 to 1750 LT. This is only a minor correction due to the discretization effect. In an analysis of the rainstorm (Junghändel et al. 2021), the most intensive time intervals are presented, corresponding to the often-used durations of 6, 12, and 24 h. The corresponding PID is 0.0191, 0.0303, and 0.0230, respectively, that is, notably less than the maximum value found for 14 h.

It should be emphasized that when one rainstorm in this analysis is referred to as greater or smaller than another, it is always based on the maximum PID that is determined from the available data on precipitation and duration. From many precipitation events, only a few related values of precipitation depth and duration are available, which makes the PID calculations very simple, but at the risk of biased results due to the Hershfield effect. This is the case for the world's largest

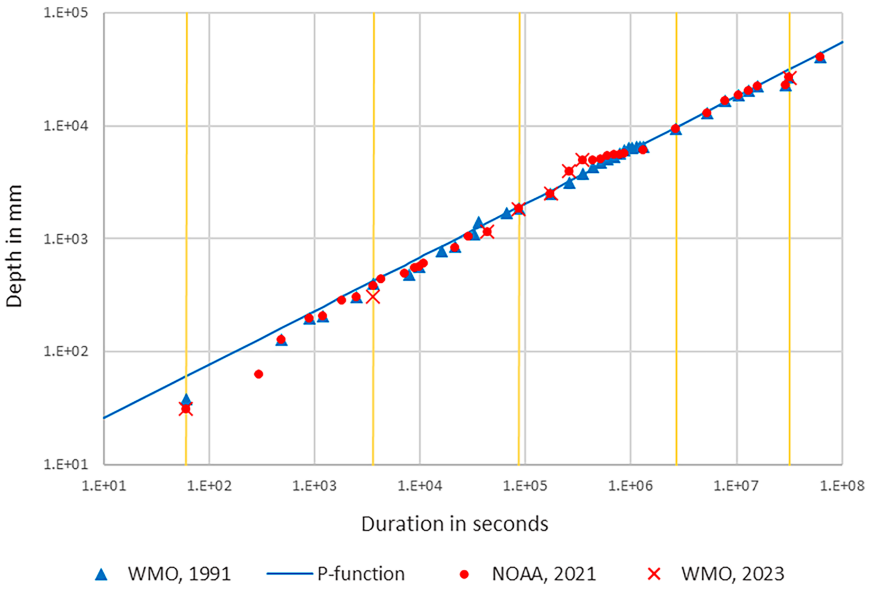

FIG. 2. World records of point rainfall. Three series of rainfall depths vs duration. The six vertical yellow lines correspond to 1 min, 1 h, 24 h, 1 month, and 1 year. The blue line is the statistically based approximation of the WMO data from 1991 (WMO 2009b).

rainfalls, which have been analyzed in the following section. Rainfall maxima determined for given time intervals (e.g., clock hours or calendar days) differ systematically from maxima determined for arbitrary time intervals of the same duration (e.g., moving time intervals of 60 min or 24 h, respectively). The Hershfield factor is a multiplier aiming to correct the error between fixed time-interval maxima and sliding maxima as a direct consequence of temporal discretization of rainfall time series (Papalexiou et al. 2016).

3. Data and results

a. Important world records of point rainfall

One of the first records of extreme rainfall was reported by Dwight (1822). In an article in *American Journal of Science and Arts*, he described "a remarkable storm which occurred at Catskill, July 26, 1819." Dwight's estimations were based on simple observations and conversations with observers, as no rain gauges were used. Despite this, Dwight's observations survived for more than 100 years. In one of the first long lists of record rainfalls (U.S. Weather Bureau 1941), Dwight's different observations were reduced to one observation: 10 in. (254 mm) in 1 h. A list from 1950 still included the Catskill storm (Jennings 1950). The differences between the two lists (1941 vs 1950) were primarily due to new observations found in the archives. This changed when the next comprehensive list as of November 1991 was compiled (WMO 2009b). Of the 37 records in that list, only 16 came from the 1950 list. The Catskill storm was replaced by another event of 401 mm of rainfall in 1 h in July 1975 in Shangdi, China. The new records were all new observations since 1950.

The newest comprehensive list as of 10 November 2021 was published by the National Oceanic and Atmospheric Administration (NOAA 2021) and has 42 records. Four of these are of questionable veracity or have yet to be considered as official records by the WMO. Two records have been surpassed by other events. Of the remaining 36 records, 14 were transferred from the 1991 list. The new records are both new observations and older ones from the archives. The relatively large difference between the 1991 and 2021 lists also reflects different choices of durations.

In Fig. 2, the three newest series are shown (NOAA 2021; WMO 2009b, 2023). All observations were from single rain gauges, that is, they represent the precipitation at a single point. Of the eight WMO records from 2023, only one differed from the records in NOAA's 2021 list. The observations from 1991 (WMO 2009b) were approximated by the equation $P = 422T^{0.475}$ (see Fig. 2), in which P is the depth in millimeters and T is the duration in hours. It is remarkable that the exponent 0.475 is so close to 0.5. This means that the world-record depths increase approximately proportionally to the square root of the durations or, as a consequence, the intensities decrease approximately inversely proportionally to the square root of the durations. This nearly square root relation has been reported by other researchers, for instance, Koutsoyiannis and Papalexiou (2017), who found an exponent of 0.48 for similar data. However, no explanation was given for this finding. In the next section, it will be shown that the square root relation is not a coincidence but rather a physical necessity.

b. Application of PID

The depth of the rainfall is the average intensity multiplied by the duration: $n = it$. Insertion of this equation in the equation for PID results in $n = (\text{PID} \times \nu)^{1/2} t^{1/2}$. A constant PID thus corresponds to a straight line with a slope coefficient of

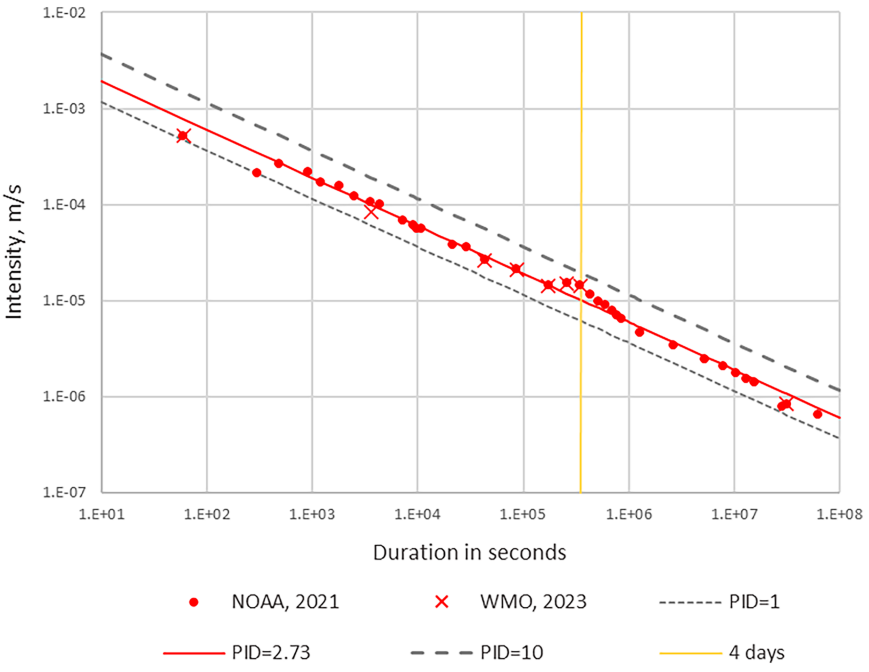

FIG. 3. Intensity vs duration compared to the PID. The red line is the mean PID of the NOAA data (NOAA 2021).

0.5 in a double logarithmic depiction of the depth n against the duration t. Similarly, the intensity is $i = (\text{PID} \times \nu)^{1/2} t^{-1/2}$, that is, a line with a slope of -0.5. In Fig. 3, the intensities of the world's greatest rainfalls are shown according to the newest lists from 2021 to 2023, along with the lines corresponding to PIDs equal to 1 and 10. Figure 3 shows that the world's greatest rainfalls have PIDs between 1 and 10, whether they last a few minutes or many months.

The mean PIDs of the five considered lists show an increasing trend: 1.48 (1941), 1.73 (1950), 2.70 (1991), 2.73 (2021), and 2.81 (2023). It is tempting to deduce that the increasing size of the mean PID is due to climate change. However, given the uncertainty associated with the data of the early lists, this conclusion is unlikely to hold. Therefore, in this analysis, the assessment of a possible climate effect is based only on the most recent lists.

If there is an upper limit for the PID, then the observed world records should be independent of the year that they were reported. To determine if this is the case, all 36 NOAA (2021) observations are sorted by their year of registration (see Fig. 4). The 16 gray dots describe PIDs from the same events. The mean of the remaining 20 independent observations (the red dots) is 2.73, that is, coincidentally the same as the mean of all 36 observations.

c. *Interpretation of results*

If only the 20 red dots in Fig. 4 are considered, all observations except three are relatively close to the mean. The largest value of 5.30, the red dot to the far right, was from 24 February 2007 on Cratère Commerson, Réunion Island, where 4.936 m of rain fell over 4 days. This rainfall event must thus be considered the greatest within documented records. This extreme rainstorm was experienced during Tropical Cyclone Gamede over Réunion Island in February 2007 (Quetelard et al. 2009). This rainfall is also indicated in Fig. 3 by the yellow line corresponding to 4 days. As already indicated in the introduction and shown in the example from Germany and the discussion of the Hershfield effect in the next section, theory, it may well be that the 4-day record rainfall starting on 24 February 2007 was surpassed (regarding the size of PID) by a rainfall over 4 days starting before or after the 24 February, or even over a shorter or longer period than just 4 days. It will be possible to find the absolute largest PID for this rainfall only with continuous measurements of precipitation (depth and or intensity) on all the days before and after the record shown here.

The magnitude of the Hershfield factor is influenced by the time scales ratio (e.g., analyzing 24 h with 1-h or 1-min time series). Typically, the Hershfield factor is a little larger than 1.1 (Papalexiou et al. 2016). Therefore, the Hershfield factor could be taken into account by increasing all records by a factor of 1.1. However, this may generally be wrong, as many of the NOAA records, in particular, are based on very specific time intervals close to each other, for example, 1, 5, 8, 15, 20, 30, 42, 60, and 72 min. Nothing here indicates that a larger precipitation should have taken place, as, for instance, a 42-min interval is not a typical time interval. When dealing with time intervals of days, months, and years, nevertheless, such corrections could make sense. But there are too few data to support such corrections.

The magnitude of the z score or coverage factor (see Joint Committee for Guides in Metrology 2008) for the 24 February 2007

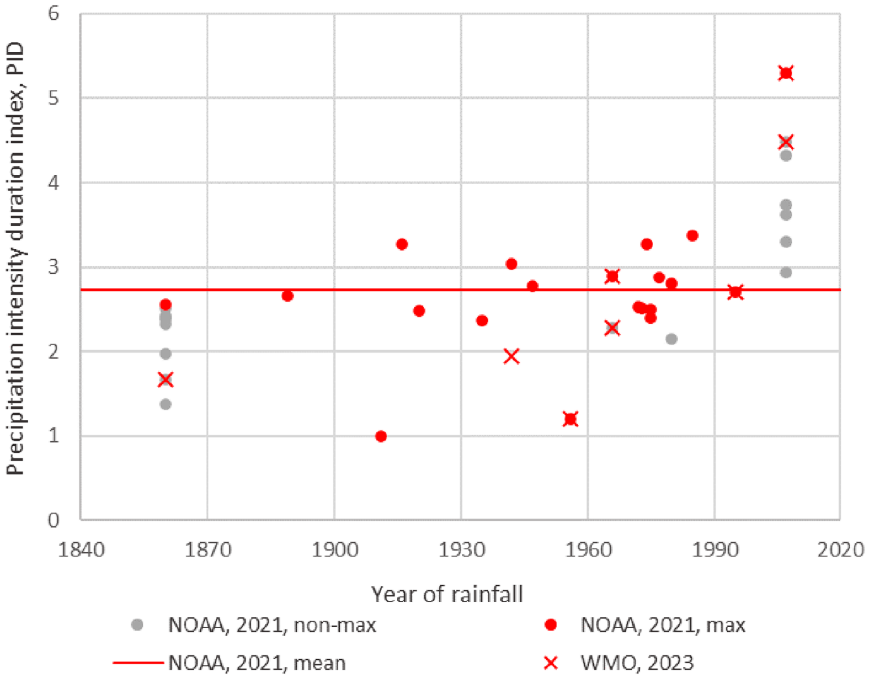

FIG. 4. PID vs the year of registration of the rainfall incident. The two-parameter description in Fig. 3 (intensity and duration) is reduced to a one-parameter description (PID), making it possible to compare rainfall events from different years of registration.

rainfall event was $(5.30 - 2.59)/0.59 = 4.60$, in which 2.59 is the mean PID of the 19 records before 2007, and 0.59 is the standard deviation of these values. Normally, a coverage factor larger than 2–3 is considered sufficient to conclude that the value differs significantly (Joint Committee for Guides in Metrology 2008). With a coverage factor of 4.60, it can be concluded that this only observation since 2000 differs significantly from all earlier observations since 1860. Usually, a single observation in a time series is not sufficient to support an alleged trend in the time series. However, the time series in Fig. 4 is not a usual time series of precipitation events from, for example, a single weather station, but instead a time series of extracted data from, in principle, all precipitation measurements across the whole Earth from the last 150 years. Therefore, a possible explanation for the extreme event in 2007 could be global warming. This is in agreement with some investigations, but in contrast to others, as described in the following paragraphs.

It is well known that the moisture capacity increases with increasing air temperature, that is, the Clausius–Clapeyron relationship, which is used in global and regional climate models. Christensen and Christensen (2004) showed, for instance, an increase in extreme summer precipitation in Europe. Alexander et al. (2006) investigated global observed changes in daily climate extremes of temperature and precipitation, showing a tendency toward wetter conditions throughout the twentieth century. Based on radar measurements, Berg et al. (2013) found that convective precipitation responds much more sensitively to temperature than does stratiform precipitation. Later investigations have also shown complex relations between warming and precipitation (see, e.g., Wang et al. 2017; Peleg et al. 2018; Papalexiou and Montanari 2019; Long et al. 2021). In a review of observational, theoretical, and modeling studies, Fowler et al. (2021) found that heavy rainfall extremes are intensifying with warming, in line with the findings of Madakumbura et al. (2021), who used machine learning methods and found anthropogenic signals in global extreme precipitation from all over the world.

However, Koutsoyiannis (2020b) found, based on spatiotemporal gridded ground observations, satellite images, and reanalysis of records of precipitation, that trends of precipitation extremes do not provide a definitive answer concerning intensification. Furthermore, Koutsoyiannis (2020b) has shown that relative humidity is, in fact, decreasing in the entire atmosphere instead of remaining constant, for which reason the specific humidity is only increasing at a rate of about one-third of that implied by the Clausius–Clapeyron model. This is in agreement with the findings of Dimitriadis et al. (2021) and Sun et al. (2012).

The two other divergent observations in Fig. 4 mentioned above, the smallest two observations with PID values close to 1.0 (from 1911 to 1956), are also the rainfall events with the largest intensities. They are seen as the two dots on the far left in Fig. 3. If the record rainfalls are considered to be the results of a so-called batch process (see appendix), then a constant PID for the world's largest rainfalls would be equivalent to all the rainfalls having had the same input (energy) available. If the intensity is very high, it is likely that some part of the available input (energy) is spilled, causing a lower intensity than what a constant PID extrapolated to very short

durations would yield. Therefore, the curve for maximum intensity (Fig. 3) may be heading toward a constant (horizontal) value for short durations. In contrast, for very long durations, the constant PID curve will cross the horizontal lines of constant intensities originating from the average intensity (yearly mean) of the wettest place on Earth (Kuttippurath et al. 2021). Therefore, the resulting course of maximum intensity is a kind of S curve with a long, straight medium section, with a constant PID until around 2000.

The eight world records from WMO (2023) are indicated by crosses in Fig. 4. As already described, only one observation differs from the dataset from NOAA (2021), namely, the 1-h rainfall event in 1947. As seen from Fig. 4, three of the WMO world records (the three red crosses on the three gray dots) are not related to the largest PID for these specific rainfall events. Therefore, in this way they are not "real" records.

4. Discussion

Heavy rainstorms play a central role in water-driven soil erosion processes (Bezak et al. 2021). Therefore, if PID is a measure of the strength of rainfall, then one should be able to find PID or terms related to PID directly or indirectly in other formulas and expressions that indicate something about the destructive abilities of rain. Two particularly important issues are considered here: soil erosion and landslides.

Rainfall erosivity, that is, the capability of a rainfall to cause soil loss, can be found by help of the widely used Universal Soil Loss Equation (USLE) and later developments herein: the Revised Universal Soil Loss Equation (RUSLE) and the latest version, RUSLE2 (Renard et al. 1997; Agricultural Research Service 2013; Nearing et al. 2017). When factors other than rainfall are held constant, soil losses from cultivated fields are, according to Renard et al. (1997), directly proportional to the total storm energy E times the maximum 30-min intensity I_{30}. The total storm energy used by RUSLE2 is $e = 0.29[1 - 0.72\exp(-0.082i)]$, in which e is the energy of the rainfall per unit rainfall depth (MJ ha^{-1} mm^{-1}), and i is the rainfall intensity (mm h^{-1}) (Nearing et al. 2017). For large intensities, which contribute most to erosion, e is seen to be almost constant, namely, 0.29. In these cases, E is nearly proportional to the rainfall depth. Therefore, the soil loss is proportional to the rainfall depth times I_{30}, that is, a quantity equivalent to the PID.

The formula for e used by RUSLE is primary empirically based. Using a consistent rainfall parameterization based on exponential distributions for the size of the raindrops, Uijlenhoet and Stricker (1999) have shown that rainfall power (storm energy per second; W m^{-2}) is related to intensity via a power law. Six different consistent sets of power-law relationships were presented, with exponents ranging between 1.06 and 1.35. The corresponding constants ranged between 2.00 and 3.01. One of the six relationships, $2.47i^{1.28}$, gives results fairly close to the corresponding results obtained using the RUSLE formula. However, all the six exponents found were greater than 1.0, which is more than the similar exponent 1.0 in the PID index. This shows that the PID index is only a rough measure for soil erosion. But it also shows that there probably are some opportunities for further modification and development of the PID index using more detailed information on, for example, raindrop size distribution.

Guzzetti et al. (2007) reviewed rainfall thresholds for the initiation of landslides worldwide and found that intensity-duration thresholds were the most common type of thresholds proposed in the literature, totaling 52 threshold equations (see Fig. 5). Of these equations, 44 were simple power laws. The equations included global thresholds, regional thresholds, and local thresholds. The types of landslides covered were mostly "all types," debris flows, and shallow landslides. Although, as noted by Guzzetti et al. (2007), global thresholds tend to be in the lower part and the local thresholds in the upper part of the figure, the variability is quite large. However, one characteristic is common for all power-law equations: the negative scaling exponent, that is, a decreasing threshold intensity for increasing duration, which Guzzetti et al. (2007) explained by a self-similar scaling behavior for the rainfall conditions that result in landslides (see also Veneziano and Lepore 2017). This self-similar scaling behavior is consistent with a constant PID, as shown in Fig. 5. Most threshold equations are located around the line corresponding to PID = 0.01. For PID below 0.001, landslides are unlikely to occur, while rainfalls with PID larger than 0.1 almost always will cause a landslide.

The analyses above are not intended as an attempt to introduce PID as an alternative to the many existing methods of describing soil erosion and landslides. The analyses and discussions are only intended to show that PID is a reasonable measure of the strength of a rainstorm.

As severe rainstorms are rarer than nonsevere rainstorms, a positive dependence between PID and the return period may be expected. Four sites from three countries are analyzed. These sites represent different climates according to the Köppen–Geiger climate classification system (Beck et al. 2018). The classifications of the four sites are as follows (with the Köppen–Geiger abbreviation shown in parentheses):

1) Wipperfürth-Gardeweg, Germany: temperate, without a dry season, warm summer (Cfb).
2) Alice Springs, Australia: arid, desert, hot (Bwh).
3) Miami, Florida: tropical, monsoon (Am).
4) Salt Lake City, Utah: on the border between cold (continental), dry summer, hot summer (Dsa) and arid, steppe, hot (Bsh).

The first site, Wipperfürth-Gardeweg, has already been introduced in the section on theory. For each site, the precipitations corresponded to 5- and 60-min durations and return periods of 10, 50, and 100 years, using the methods and data specified by DWD (2022), the Bureau of Meteorology (2023), and NOAA (2023). The resulting PIDs are shown in Fig. 6.

The expected positive relation between PID and the return period at a given site is clearly shown in Fig. 6. However, what is more interesting is that this dependence is much weaker than the dependence on location, that is, the climate classification. For instance, the PID value for a 100-yr, 5-min storm event in Alice Springs is nearly 10 times larger than for an equivalent storm event in Salt Lake City, and the PID

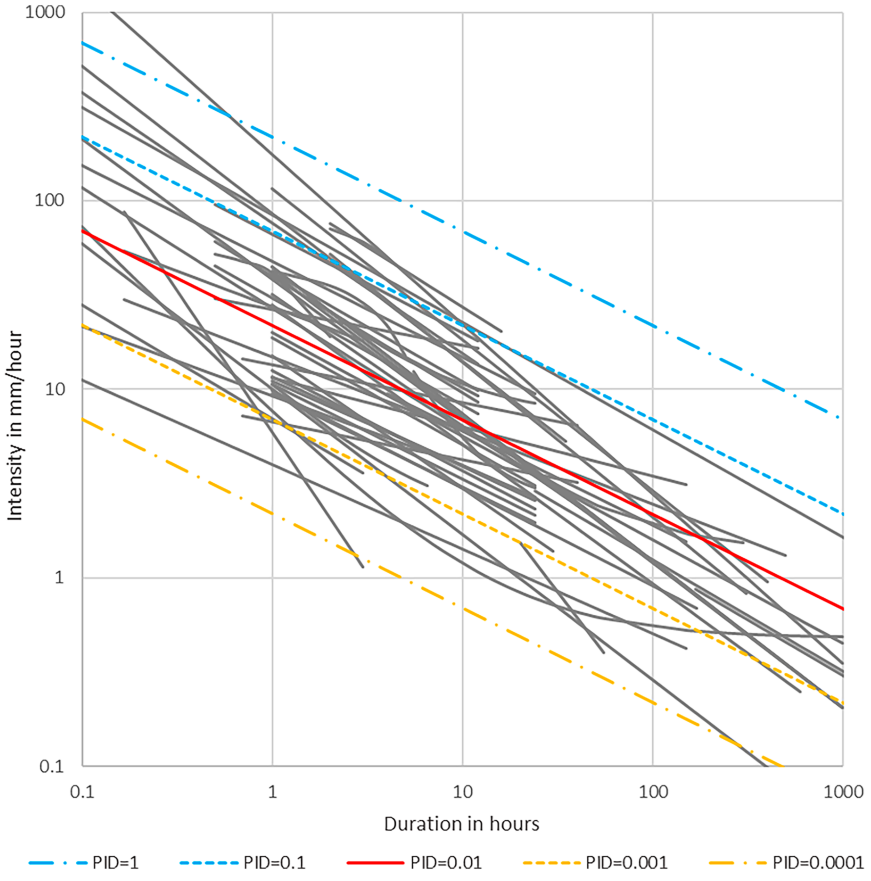

FIG. 5. The gray lines show 52 rainfall intensity–duration thresholds based on Table 2 in Guzzetti et al. (2007). The colored lines are constant PIDs.

value in Miami is about 2.5 times larger than in Alice Springs. In Miami, 60-min storms are more severe (larger PID) than the 5-min storms, while the opposite is true in Salt Lake City. In Alice Springs, the two curves overlap, and both overlap the 5-min curve from Germany. This rather confusing pattern shows that, as already implied in the introduction, there is no unambiguous connection between PID and the 100-yr events, for example. Therefore, it is not useful to compare world records using return periods, recurrence intervals, or IDF curves.

If rainstorms in geographical areas of limited extent are analyzed, the use of return periods will, of course, be entirely relevant. This was what Ceresetti et al. (2012) did in their study of three major storms that occurred over a mountainous Mediterranean region of southern France, using maximum intensity diagrams and severity diagrams. The first diagram displays the maximum rainfall intensities as a function of time (duration in hours) and surface area (in km^2), while the others, called the severity diagrams, display the corresponding return periods, again as a function of time and area. The use of severity diagrams requires knowledge of the extreme rainfall distribution in the region. An alternative or supplementary severity diagram is to show PID as a function of time and area, which can be constructed simply using the durations and the intensities from the intensity diagrams. Such PID contour diagrams can also be used to describe a single event over a large area, such as the catastrophic rainstorm in central Europe in July 2021. The "volume" under the PID contour surface is a measure of the severity of the whole incident.

Finally, it should be noted that the PID value (0.035) for the torrential rainfall in Germany in July 2021 is only less than 1% of the maximum PID value worldwide, that is, PID = 5.30 from 24 February 2007 on Cratère Commerson, Réunion Island. However, the event in central Europe in 2021 caused more than 200 fatalities in Germany and Belgium (Magnusson et al. 2021), while only one person was killed on Réunion Island in 2007 (ESA 2023). This shows that not only the magnitude of the strength of the individual rainfall event (the size of PID) but also the geographical extent of the rainfall event, the geology of the area, and the population density, among other factors, determine the consequences. The PID is a measure of only the strength of a point precipitation.

5. Conclusions

By applying dimensional analysis, it has been shown that an important parameter to characterize rainfall is the PID, a new dimensionless number. Observations from around the world

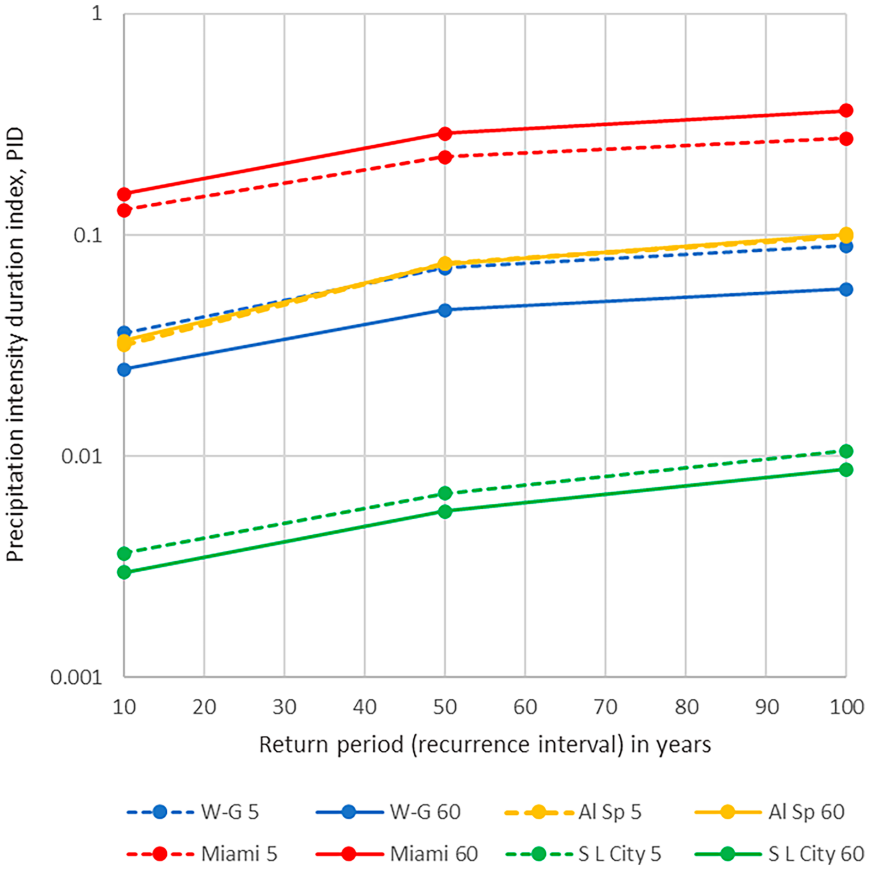

FIG. 6. PID as a function of the return period from four sites around the world: Wipperfürth-Gardeweg, Germany (W-G); Alice Springs, Australia (Al Spa); Miami; and Salt Lake City (S L City). The durations (min) are indicated by 5 and 60. Data are from DWD (2022), Bureau of Meteorology (2023), and NOAA (2023).

show that the world's greatest point rainfalls have approximately the same PID, with an average PID of 2.73. This value covers rainfall lasting from 1 min to 2 years. As a result, the intensity of all these recorded rainfalls is inversely proportional to the square root of the duration. A simple physical explanation for this relation could be that all these maximum rainfall events have had the same amount of available input (energy).

The application of the PID makes it possible to compare different point-rainfall events in a way that has never been done before, for instance, in time. One rainfall event differs from all other rainfall events since 1860, which is the 4-day rainfall event starting on 24 February 2007 on Cratère Commerson, Réunion Island, described by Quetelard et al. (2009). This rainfall event has the largest PID and thus must be considered the world's largest rainstorm within documented records.

Acknowledgments. The author is very grateful to Dr. Wade T. Crow, the Chief Editor of the *Journal of Hydrometeorology*, and the four reviewers, especially Professor Dr. Remko Uijlenhoet, for their very helpful suggestions in improving this article.

Data availability statement. The five rainfall datasets of world records used in this study are available from open-access sources as follows: 1941 data are from U.S. Weather Bureau (1941), 1950 data are from Jennings (1950), 2009 data are from WMO (2009b), 2021 data are from NOAA (2021), and 2022 data are from WMO (2023). The data used in Fig. 1 are from DWD (2023). The data used in Fig. 5 are from Table 2 in Guzzetti et al. (2007). The data used in Fig. 6 are from DWD (2022), Bureau of Meteorology (2023), and NOAA (2023).

APPENDIX

Batch Process Analogy

In the process industry, a batch process is a process with a well-defined beginning and end, similar to a rainstorm. A rainstorm can be thought of as a "rainfall machine" that, with the input Q_i, "produces" the output $Q_u = n$ meters of precipitation with an intensity of $i = n/t$. In a batch process, Q_i is the known amount of energy and raw materials. In the case of a rainstorm, we can measure related values of n and t, but we do not know Q_i. However, thinking of Q_i as a sort of "energy" can be helpful.

A well-known example of a batch process involves driving a car that travels at a constant speed v, which is equivalent to the intensity of the rainfall. Before starting the car, the tank (or battery) is filled with Q_i joules. The car travels a distance of x meters in t seconds until the tank runs out of energy. Likewise, the rain reaches a rainfall depth of n meters. The speed, therefore, has been $v = x/t$ or, for the rainfall, $i = n/t$, which is called the time productivity (i.e., output per unit of time) or simply the process speed in this process. Productivity can also be related to the input, that is, measured as the output per input. The reciprocal value of this productivity is the input consumption per meter driven or per meter depth of rainfall:

$$e_n = Q_i/n, \tag{A1}$$

where e_n will usually depend on the process speed; thus, the greater the speed is, the greater the input consumption per unit produced. The input consumption is assumed to be proportional to the process speed to the power of h:

$$e_n = e_B(i/i_B)^h, \tag{A2}$$

where h is a dimensionless exponent, and e_B is the input consumption corresponding to the reference intensity i_B. This means that $C_B = i_B^h/e_B$ is a constant. As a simple illustration, a moving object is considered. If the object is pulled on a horizontal plane, the friction force is constant, which is why $h = 0$. For an object moving through a liquid, $h = 1$ in the case of laminar flow and $h = 2$ in the case of turbulent flow. For a moving car, h will be approximately 1 for low speeds and approximately 2 for high speeds.

The input consumption per unit time (power) is e_n times the intensity (velocity):

$$e_t = (e_B/i_B^h)i^{1+h}. \tag{A3}$$

Introducing a characteristic precipitation, $n_B = Q_i/e_B$, and a characteristic time, $t_B = n_B/i_B$, in (A1) and (A2) leads to the following expressions of the relationships between precipitation and time and intensity and time, respectively:

$$n/n_B = (t/t_B)^{h/(1+h)}, \tag{A4}$$

$$i/i_B = (t/t_B)^{-1/(1+h)}. \tag{A5}$$

The PID can be found from (A4) and (A5):

$$\mathrm{PID} = in/v = i_B n_B/v(t/t_B)^{(h-1)/(h+1)}. \tag{A6}$$

For the world's greatest rainstorms, it has been shown that PID is nearly constant regardless of the duration of the storm. This means that (A6) must be independent of t, which is met for $h = 1$. If the hypothesis of the large rainfall machine is accepted, $h = 1$ corresponds to the fact that laminar forces are dominant. Then, PID is

$$\mathrm{PID} = in/v = i_B n_B/v = C_B Q_i/v. \tag{A7}$$

As Q_i and v are constants, the PID, that is, the strength of the rainstorm, is directly proportional to the amount of input (energy). It seems likely that the maximum amount of input may increase in the coming years due to a warming climate, that is, no physical upper limit exists for precipitation. This is consistent with the findings in Fig. 4 and the analyses of Koutsoyiannis and Papalexiou (2017).

The two points on the far left in Fig. 3 seem to support that the intensity approaches a constant value for durations going toward zero. Therefore, the PID is not constant for these incidents but decreases for short durations. The mean precipitation at one of the wettest spots on Earth, Mawsynram in India, was 12.55 m yr^{-1} for the 1989–2010 period (Kuttippurath et al. 2021). This corresponds to an average intensity of 3.98×10^{-7} m s^{-1}. The mean PID curve, the red line in Fig. 3, crosses this intensity for $t = 2.30 \times 10^{-8}$ s, or 7.28 years. This shows that the curve for maximal intensities also approaches a constant value for very long durations.

An explanation of these two border cases can be provided by the analogy of the batch process of driving a car. A constant PID corresponds, as mentioned, to the fact that the rainfall machine starts with a filled tank and rains (runs) until the tank runs out. The rainfall machine, like any other machine, must necessarily have an upper limit of the engine's maximum power. No matter how much fuel is added into the car's engine, it will not be able to provide more than that maximum power. The gas will just go to waste. The result is a horizontal course of maximum intensity for short times. Conversely, if the car is constantly supplied with a tiny amount of fuel, it will never completely grind to a halt but will continue at a modest speed, no matter how much time passes. That is, again, a horizontal course of the speed, that is, the intensity corresponding to the wettest place on Earth. The resulting form of the maximum intensity curve (Fig. 3) is, therefore, a kind of S curve.

The hypothesis that the world's largest rainfalls all have had the same total input consumption, corresponding to the same PID, seems underpinned by theory and observations. However, the observations from 2007 also point to a possible increasing trend of the maximum PID, which may be due to climate change. The total amount of input (energy) available is, therefore, perhaps, increasing. Global warming resulting in increasing evaporation, that is, intensification of the hydrologic cycle, is reflected in increasing stratification, as observed recently by satellite sea surface salinity measurements (Olmedo et al. 2022).

REFERENCES

Agricultural Research Service, 2013: Science documentation revised universal soil loss equation version 2 (RUSLE2). USDA, 355 pp., https://www.ars.usda.gov/ARSUserFiles/60600505/rusle/rusle2_science_doc.pdf.

Alexander, L. V., and Coauthors, 2006: Global observed changes in daily climate extremes of temperature and precipitation. *J. Geophys. Res.*, **111**, D05109, https://doi.org/10.1029/2005JD006290.

Beard, K. V., 1976: Terminal velocity and shape of cloud and precipitation drops aloft. *J. Atmos. Sci.*, **33**, 851–864, https://doi.org/10.1175/1520-0469(1976)033<0851:TVASOC>2.0.CO;2.

Beck, H., N. E. Zimmermann, T. R. McVicar, N. Vergopolan, A. Berg, and E. F. Wood, 2018: Present and future Köppen-Geiger climate classification maps at 1-km resolution. *Sci. Data*, **5**, 180214, https://doi.org/10.1038/sdata.2018.214.

Berg, P., C. Moseley, and J. O. Haerter, 2013: Strong increase in convective precipitation in response to higher temperatures. *Nat. Geosci.*, **6**, 181–185, https://doi.org/10.1038/ngeo1731.

Bernard, M. M., 1932: Formulas for rainfall intensities of long duration. *Trans. Amer. Soc. Civ. Eng.*, **96**, 592–624, https://doi.org/10.1061/TACEAT.0004323.

Beven, K., 2021: Issues in generating stochastic observables for hydrological models. *Hydrol. Processes*, **35**, e14203, https://doi.org/10.1002/hyp.14203.

Bezak, N., M. Mikos, P. Borrelli, L. Liakos, and P. Panagos, 2021: An in-depth statistical analysis of the rainstorms erosivity in Europe. *CATENA*, **206**, 105577, https://doi.org/10.1016/j.catena.2021.105577.

Bohr, N., 1913: On the constitution of atoms and molecules. *London Edinburgh Dublin Philos. Mag. J. Sci.*, **26** (151), 1–25, https://doi.org/10.1080/14786441308634955.

Buckingham, E., 1914: On physically similar systems; illustrations of the use of dimensional equations. *Phys. Rev.*, **4**, 345–376, https://doi.org/10.1103/PhysRev.4.345.

Bureau of Meteorology, 2023: Design rainfalls. Bureau of Meteorology, Australian Government, accessed 12 January 2023, http://www.bom.gov.au/water/designRainfalls/index.shtml.

Caskey, J. E., 1963: A Markov chain model for the probability of precipitation occurrence in intervals of various length. *Mon. Wea. Rev.*, **91**, 298–301, https://doi.org/10.1175/1520-0493(1963)091<0298:AMCMFT>2.3.CO;2.

Ceresetti, D., S. Anquetin, and G. Molinié, 2012: Multiscale evaluation of extreme rainfall event predictions using severity diagrams. *Wea. Forecasting*, **27**, 174–188, https://doi.org/10.1175/WAF-D-11-00003.1.

Cerveny, R., 2018: WMO archive of weather and climate extremes. *WMO Bull.*, **67**, 52–57.

Chang, T. J., M. L. Kavvas, and J. W. Delleur, 1984: Daily precipitation modelling by discrete autoregressive moving average processes. *Water Resour. Res.*, **20**, 565–580, https://doi.org/10.1029/WR020i005p00565.

Chow, V. T., D. R. Maidment, and L. W. Mays, 1988: *Applied Hydrology*. McGraw-Hill, 294 pp.

Christensen, O. B., and J. H. Christensen, 2004: Intensification of extreme European summer precipitation in a warmer climate. *Global Planet. Change*, **44**, 107–117, https://doi.org/10.1016/j.gloplacha.2004.06.013.

Dahamsheh, A., and H. Aksoy, 2009: Artificial neural network models for forecasting intermittent monthly precipitation in arid regions. *Meteor. Appl.*, **16**, 325–337, https://doi.org/10.1002/met.127.

Dimitriadis, P., D. Koutsoyiannis, T. Iliopoulou, and P. Papanicolaou, 2021: A global-scale investigation of stochastic similarities in marginal distribution and dependence structure of key hydrological-cycle processes. *Hydrology*, **8**, 59, https://doi.org/10.3390/hydrology8020059.

DWD, 2022: Grids of return periods of heavy precipitation (design precipitation) over Germany (KOSTRA_DWD), version 2010R and 2020. DWD Climate Data Center, accessed 12 October 2022, https://opendata.dwd.de/climate_environment/CDC/grids_germany/return_periods/precipitation/KOSTRA/.

——, 2023: Precipitation data from Wipperfürth-Gardeweg: Observations_germany/, Climate, hourly, precipitation, historical, stundenwerte_RR-05619_20041201_20221231_hist.zip. DWD Climate Data Center Open Data Server, accessed 20 April 2023, https://cdc.dwd.de/portal/.

Dwight, B. W., 1822: An account of a remarkable storm which occurred at Catskill, July 26, 1819. *Amer. J. Sci. Arts*, **4**, 124–142.

ESA, 2023: Cyclone Gamede (Reunion)—March 2007. European Space Agency Earth Watching project, accessed 23 April 2023, https://earth.esa.int/web/earth-watching/natural-disasters/cyclones/cyclone-events/-/asset_publisher/4Lfz/content/cyclone-gamede-reunion-march-2007/.

Fowler, H. J., and Coauthors, 2021: Anthropogenic intensification of short-duration rainfall extremes. *Nat. Rev. Earth Environ.*, **2**, 107–122, https://doi.org/10.1038/s43017-020-00128-6.

Gabriel, K. R., and J. Neumann, 1962: A Markov chain model for daily rainfall occurrence at Tel Aviv. *Quart. J. Roy. Meteor. Soc.*, **88**, 90–95, https://doi.org/10.1002/qj.49708837511.

Gámez-Balmaceda, E., A. López-Ramos, L. Martínez-Acosta, J. P. Medrano-Barboza, J. F. R. López, G. Seingier, L. W. Daesslé, and A. A. López-Lambraño, 2020: Rainfall intensity-duration-frequency relationship. Case study: Depth-duration ratio in a semi-arid zone in Mexico. *Hydrology*, **7**, 78, https://doi.org/10.3390/hydrology7040078.

Genest, C., and F. Chebana, 2017: Copula modelling in hydrologic frequency analysis. *Handbook of Applied Hydrology*, V. P. Singh, Ed., McGraw Hill, 30.1–30.10.

Gregersen, I. B., H. Madsen, J. J. Linde, and K. Arnbjerg-Nielsen, 2014: Updated climate factors and design rain intensities (in Danish). IDA Waste Water Committee Paper 30, 32 pp., https://spildevandskomiteen.dk/wp-content/uploads/svk_skrift30_0.pdf.

Grimaldi, S., and F. Serinaldi, 2006: Design hyetograph analysis with 3-copula function. *Hydrol. Sci. J.*, **51**, 223–238, https://doi.org/10.1623/hysj.51.2.223.

Guzzetti, F., S. Peruccacci, M. Rossi, and C. P. Stark, 2007: Rainfall thresholds for the initiation of landslides in central and southern Europe. *Meteor. Atmos. Phys.*, **98**, 239–267, https://doi.org/10.1007/s00703-007-0262-7.

Hannachi, A., 2012: Intermittency, autoregression and censoring: A first-order AR model for daily precipitation. *Meteor. Appl.*, **21**, 384–397, https://doi.org/10.1002/met.1353.

Hecksher, T., 2017: Insights through dimensions. *Nat. Phys.*, **13**, 1026, https://doi.org/10.1038/nphys4285.

Iliopoulou, T., and D. Koutsoyiannis, 2019: Revealing hidden persistence in maximum rainfall records. *Hydrol. Sci. J.*, **64**, 1673–1689, https://doi.org/10.1080/02626667.2019.1657578.

Jennings, A. H., 1950: World's greatest observed point rainfalls. *Mon. Wea. Rev.*, **78**, 4–5, https://doi.org/10.1175/1520-0493(1950)078<0004:WGOPR>2.0.CO;2.

Johnson, F., and A. Sharma, 2017: Design rainfall. *Handbook of Applied Hydrology*, V. P. Singh, Ed., McGraw Hill, 125.3–125.13.

Joint Committee for Guides in Metrology, 2008: Evaluation of measurement data—Guide to the expression of uncertainty in measurement, GUM 1995 with minor corrections. 134 pp., https://www.bipm.org/documents/20126/2071204/JCGM_100_2008_E.pdf.

Junghändel, T., and Coauthors, 2021: Hydro-klimatologische Einordnung der Stark-und Dauerniederschläge in Teilen Deutschlands im Zusammenhang mit dem Tiefdruckgebiet "Bernd" vom 12. bis 19. Juli 2021. DWD Geschäftsbereich Klima und Wetter, accessed 21 July 2021, https://www.dwd.de/DE/leistungen/besondereereignisse/niederschlag/20210721_bericht_starkniederschlaege_tief_bernd.html.

Katz, R. W., and M. B. Parlange, 1998: Overdispersion phenomenon in stochastic modelling of precipitation. *J. Climate*, **11**, 591–601, https://doi.org/10.1175/1520-0442(1998)011<0591:OPISMO>2.0.CO;2.

Keifer, C. J., and H. H. Chu, 1957: Synthetic storm pattern for drainage design. *J. Hydraul. Div.*, **83** (4), 1–25, https://doi.org/10.1061/JYCEAJ.0000104.

Koutsoyiannis, D., 2000: A generalized mathematical framework for stochastic simulation and forecast of hydrologic time series. *Water Resour. Res.*, **36**, 1519–1533, https://doi.org/10.1029/2000WR900044.

——, 2004a: Statistics of extremes and estimation of extreme rainfall: I. Theoretical investigation. *Hydrol. Sci. J.*, **49**, 575–590, https://doi.org/10.1623/hysj.49.4.575.54430.

——, 2004b: Statistics of extremes and estimation of extreme rainfall, 2, Empirical investigation of long rainfall records. *Hydrol. Sci. J.*, **49**, 591–610, https://doi.org/10.1623/hysj.49.4.591.54424.

——, 2005: Uncertainty, entropy, scaling and hydrological stochastics. 1. Marginal distributional properties of hydrological processes and state scaling. *Hydrol. Sci. J.*, **50**, 381–404, https://doi.org/10.1623/hysj.50.3.381.65031.

——, 2006: An entropic-stochastic representation of rainfall intermittency: The origin of clustering and persistence. *Water Resour. Res.*, **42**, W01401, https://doi.org/10.1029/2005WR004175.

——, 2016: Generic and parsimonious stochastic modelling for hydrology and beyond. *Hydrol. Sci. J.*, **61**, 225–244, https://doi.org/10.1080/02626667.2015.1016950.

——, 2020a: Simple stochastic simulation of time irreversible and reversible processes. *Hydrol. Sci. J.*, **65**, 536–551, https://doi.org/10.1080/02626667.2019.1705302.

——, 2020b: Revisiting the global hydrological cycle: Is it intensifying? *Hydrol. Earth Syst. Sci.*, **24**, 3899–3932, https://doi.org/10.5194/hess-24-3899-2020.

——, 2022: *Stochastics of Hydroclimatic Extremes—A Cool Look at Risk*. 2nd ed. Kallipos Open Academic Editions, 346 pp., https://doi.org/10.57713/kallipos-1.

——, and S. M. Papalexiou, 2017: Extreme rainfall: Global perspective. *Handbook of Applied Hydrology*, V. P. Singh, Ed., McGraw Hill, 74.1–74.16.

——, D. Kozonis, and A. Manetas, 1998: A mathematical framework for studying rainfall intensity-duration-frequency relationships. *J. Hydrol.*, **206**, 118–135, https://doi.org/10.1016/S0022-1694(98)00097-3

Kuttippurath, J. S., and Coauthors, 2021: Observed rainfall changes in the past century (1901–2019) over the wettest place on Earth. *Environ. Res. Lett.*, **16**, 024018, https://doi.org/10.1088/1748-9326/abcf78.

Lombardo, F., E. Volpi, D. Koutsoyiannis, and F. Serinaldi, 2017: A theoretically consistent stochastic cascade for temporal disaggregation of intermittent rainfall. *Water Resour. Res.*, **53**, 4586–4605, https://doi.org/10.1002/2017WR020529.

Long, K., D. Wang, G. Wang, J. Zhu, S. Wang, and S. Xie, 2021: Higher temperature enhances spatiotemporal concentration of rainfall. *J. Hydrometeor.*, **22**, 3159–3169, https://doi.org/10.1175/JHM-D-21-0034.1.

Madakumbura, G. D., C. W. Thackeray, J. Norris, N. Goldenson, and A. Hall, 2021: Anthropogenic influence on extreme precipitation over global land areas seen in multiple observational datasets. *Nat. Commun.*, **12**, 3944, https://doi.org/10.1038/s41467-021-24262-x.

Magnusson, L., A. Simmons, S. Harrigan, and F. Pappenberger, 2021: Extreme rain in Germany and Belgium in July 2021. *ECMWF Newsletter*, No. 169, ECMWF, Reading, United Kingdom, 2–3, https://www.ecmwf.int/en/elibrary/81276-newsletter-no-169-autumn-2021.

Martel, J.-L., F. P. Brissette, P. Lucas-Picher, M. Troin, and R. Arsenault, 2021: Climate change and rainfall intensity–duration–frequency curves: Overview of science and guidelines for adaptation. *J. Hydrol. Eng.*, **26**, 031231001, https://doi.org/10.1061/(ASCE)HE.1943-5584.0002122.

Mukhopadhyay, B., and W. Kappel, 2017: Probable maximum precipitation. *Handbook of Applied Hydrology*, V. P. Singh, Ed., McGraw Hill, 126.1–126.18.

Nearing, M. A., S. Yin, P. Borelli, and V. O. Polyakov, 2017: Rainfall erosivity: An historical review. *CATENA*, **157**, 357–362, https://doi.org/10.1016/j.catena.2017.06.004.

NOAA, 2021: HSDC World Point Precipitation Measurements. NOAA/NWS, accessed 10 December 2021, https://www.weather.gov/owp/hdsc_world_record.

——, 2023: Precipitation Frequency Data Server (PFDS). NOAA/NWS, accessed 12 January 2023, https://hdsc.nws.noaa.gov/hdsc/pfds/.

Olmedo, E., and Coauthors, 2022: Increasing stratification as observed by satellite sea surface salinity measurements. *Sci. Rep.*, **12**, 6279, https://doi.org/10.1038/s41598-022-10265-1.

Papalexiou, S. M., 2018: Unified theory for stochastic modelling of hydroclimatic processes: Preserving marginal distributions, correlation structures, and intermittency. *Adv. Water Resour.*, **115**, 234–252, https://doi.org/10.1016/j.advwatres.2018.02.013.

——, and A. Montanari, 2019: Global and regional increase of precipitation extremes under global warming. *Water Resour. Res.*, **55**, 4901–4914, https://doi.org/10.1029/2018WR024067.

——, Y. G. Dialynas, and S. Grimaldi, 2016: Hershfield factor revisited: Correcting annual maximum precipitation. *J. Hydrol.*, **542**, 884–895, https://doi.org/10.1016/j.jhydrol.2016.09.058.

Peleg, N., P. Burlando, A. Sharma, E. Morin, P. Molnar, S. Fatichi, and F. Marra, 2018: Intensification of convective rain cells at warmer temperatures observed from high-resolution weather radar data. *J. Hydrometeor.*, **19**, 715–726, https://doi.org/10.1175/JHM-D-17-0158.1.

Quetelard, H., P. Bessemoulin, R. S. Cerveny, T. C. Peterson, A. Burton, and Y. Boodhoo, 2009: Extreme weather: World-record rainfalls during Tropical Cyclone Gamede. *Bull. Amer. Meteor. Soc.*, **90**, 603–608, https://doi.org/10.1175/2008BAMS2660.1.

Renard, K. G., G. R. Foster, G. A. Weesies, D. K. McCool, and D. C. Yoder, 1997: *Predicting Soil Erosion by Water: A Guide to Conservation Planning with the Revised Universal Soil Loss Equation (RUSLE)*. U.S. Department of Agriculture, Agriculture Handbook 703, 404 pp.

Reynolds, O., 1883: An experimental investigation of the circumstances which determine whether the motion of water shall be direct or sinuous, and of the law of resistance in parallel channels. *Philos. Trans. Roy. Soc.*, **174**, 935–982, https://doi.org/10.1098/rstl.1883.0029.

Rosbjerg, D., and H. Madsen, 2019: Initial design of urban drainage systems for extreme rainfall events using intensity–duration–area (IDA) curves and Chicago design storms (CDS). *Hydrol. Sci. J.*, **64**, 1397–1403, https://doi.org/10.1080/02626667.2019.1645958.

Schoof, J. T., and S. C. Pryor, 2008: On the proper order of Markov chain model for daily precipitation occurrence in the

contiguous United States. *J. Appl. Meteor. Climatol.*, **47**, 2477–2486, https://doi.org/10.1175/2008JAMC1840.1.

Sun, F., M. L. Roderick, and G. D. Farquhar, 2012: Changes in the variability of global land precipitation. *Geophys. Res. Lett.*, **39**, L19402, https://doi.org/10.1029/2012GL053369.

Sun, Y., D. Wendi, D. E. Kim, and S.-Y. Liong, 2019: Deriving intensity–duration–frequency (IDF) curves using downscaled in situ rainfall assimilated with remote sensing data. *Geosci. Lett.*, **6**, 17, https://doi.org/10.1186/s40562-019-0147-x.

Uijlenhoet, R., and J. N. M. Stricker, 1999: A consistent rainfall parameterization based on the exponential raindrop size distribution. *J. Hydrol.*, **218**, 101–127, https://doi.org/10.1016/S0022-1694(99)00032-3.

U.S. Weather Bureau, 1941: The record rainfalls of the world. *Mon. Wea. Rev.*, **69**, 356–35, https://doi.org/10.1175/1520-0493(1941)069<0356:TRROTW>2.0.CO;2.

Veneziano, D., and C. Lepore, 2017: Scaling and fractals. *Handbook of Applied Hydrology*, V. P. Singh, Ed., McGraw Hill, 28.1–28.6.

Wang, G., D. Wang, K. E. Trenberth, A. Erfanian, M. Yu, and G. Michael, 2017: The peak structure and future changes of the relationships between extreme precipitation and temperature. *Nat. Climate Change*, **7**, 268–274, https://doi.org/10.1038/nclimate3239.

Wenzel, H. G., 1982: Rainfall for urban stormwater design. *Urban Stormwater Hydrology*, *Water Resources Monogr.*, Vol. 7, Amer. Geophys. Union, 35–67.

Wiuff, R., 2020: Analysis and modelling of precipitation intermittency by compound Markov-DARMA models. *Water Resour. Res.*, **56**, e2019WR025522, https://doi.org/10.1029/2019WR025522.

WMO, 2009a: Manual on Estimation of Probable Maximum Precipitation (PMP). WMO-1045, 291 pp., https://library.wmo.int/doc_num.php?explnum_id=7706.

——, 2009b: Management of Water Resources and Application of Hydrological Practices. Vol. II, Guide to Hydrological Practices, 6th ed. WMO-168, II.5–I19, 302 pp., https://library.wmo.int/index.php?lvl=notice_display&id=543#.YgKXbepKhPY.

——, 2021: Measurements of Meteorological Variables. Vol. I, Guide to Instruments and Methods of Observation, WMO-8, 581 pp., https://library.wmo.int/doc_num.php?explnum_id=11386.

——, 2023: World Meteorological Organization global weather & climate extremes archive. WMO, accessed 19 January 2023, https://wmo.asu.edu/content/world-meteorological-organization-global-weather-climate-extremes-archive.